Available online at www.sciencedirect.com
SCIENCE DIRECT®
Solid State Sciences 4 (2002) 1273–1283
Solid State Sciences
www.elsevier.com/locate/ssscie

Magnetic structure and exchange interactions in $CuFe_2(P_2O_7)_2$

N. El Khayati [a,b], J. Rodríguez-Carvajal [a,*], F. Bourée [a], T. Roisnel [a], R. Cherkaoui [b], A. Boutfessi [c], A. Boukhari [c]

[a] *Laboratoire Léon Brillouin (CEA-CNRS), CEA/Saclay, 91191 Gif sur Yvette cedex, France*
[b] *Département de physique, faculté des sciences, av. Ibn Batouta, B.P. 1014, Rabat, Morocco*
[c] *Laboratoire de chimie du solide appliquée, faculté des sciences, av. Ibn Batouta, B.P. 1014, Rabat, Morocco*

Received 26 July 2002; accepted 4 September 2002

Abstract

The compound $CuFe_2(P_2O_7)_2$ crystallises in the monoclinic system with space group $P2_1/n$. The crystal structure is characterised by the presence of centrosymmetric Fe–Cu–Fe trimers with intra-trimer superexchange interactions. The magnetic interactions between trimers occur through super-superexchange paths consisting of PO_4 groups connecting the trimers formed by FeO_6 octahedra and square planar CuO_4 groups. Susceptibility measurements indicate an antiferromagnetic behaviour at low temperature. Neutron powder diffraction confirms this and the determined Néel temperature is $T_N = 15.5(5)$ K. The propagation vector of the magnetic structure is $\mathbf{k} = (1/2, 0, 1/2)$, the ions inside a trimer are coupled ferromagnetically and the magnetic moments are all oriented along the b axis. The value of the staggered moments at 1.5 K are 0.83(6) and 4.88(4) μ_B for Cu^{2+} and Fe^{3+} ions, respectively. The conditions to be satisfied by the exchange interactions in order to get the observed magnetic structure as the stable ground state are discussed.

Keywords: Iron–copper pyrophosphate; Neutron diffraction; Magnetic structure; Super-superexchange interactions; Magnetic phase diagram

1. Introduction

We are interested in the magnetic properties of phosphates having coexisting M–O–M′ superexchange with super-superexchange (M–O–O–M′) magnetic interactions mediated by phosphate groups (MO_n–PO_4–$M'O_m$). Our ultimate aim is to investigate the relative strength of the exchange integrals in these materials and the consistency with the empirical Goodenough–Kanamori–Anderson rules for the superexchange interactions in insulators. For that end we need, as the first step, the determination of the magnetic structure of the studied phosphate materials. Neutron powder diffraction is the technique of choice for such a kind of investigations and we have used it for the study of different compounds presenting magnetic order at low temperatures [1–3]. In this paper we are concerned with one of these materials: $CuFe_2(P_2O_7)_2$. This compound crystallises in the monoclinic system with space group $P2_1/n$, $Z = 2$, and cell parameters $a = 6.5921(3)$ Å; $b = 5.1606(2)$ Å; $c = 15.6397(5)$ Å and $\beta = 91.983(3)^\circ$ at room temperature. The structure is formed by CuO_4, FeO_6 and PO_4 groups connected by vertices. The oxygen atoms forming the square planar groups CuO_4 are shared with four PO_4 tetrahedra belonging to two P_2O_7 groups. From the magnetic point of view, the crystal structure is characterised by the presence of centrosymmetric Fe–Cu–Fe trimers with intra-trimer superexchange interactions (near 90°: Cu–O–Fe double paths). The magnetic interactions between different trimers are of the super-superexchange type involving, at least, two oxygen atoms in the exchange paths. The structure of $CuFe_2(P_2O_7)_2$ constitutes a new structural type recently found in the phosphates of general formula $A^{II}B_2^{III}(P_2O_7)_2$ [4]. As we shall see below the magnetic topology of the magnetic atoms in this material has a potential high degree of frustration due to the presence of triangular layers of Fe^{3+} ions. After determining the magnetic structure we have performed numerical calculations in order to get insight into the relative strength of the exchange interactions responsible for the observed magnetic ground state. To perform the calculations we have considered only isotropic exchange interactions, because anisotropy is expected to be relatively weak and contributes merely to orient the whole spin configuration with respect to the crystal lattice.

* Correspondence and reprints.

1293-2558/02/$ – see front matter
PII: S1293-2558(02)00015-8

The paper is organised as follows: in Section 2 we describe the procedure for the synthesis and the experiments performed on the sample; in Section 3 the results obtained by magnetic measurements, the refinement of the crystal and magnetic structures are described in detail; in Section 4 we discuss the results concerning the magnetic structure, we analyse the geometrical features of the different exchange paths and propose a hierarchy of isotropic superexchange and super-superexchange interactions in order to obtain the observed magnetic structure as the ground state; finally, in Section 5, we summarise our conclusions.

2. Experimental

Powder of $CuFe_2(P_2O_7)_2$ was synthesised by mixing stoichiometric amounts of CuO, Fe_2O_3 and $(NH_4)_2HPO_4$, according to the reaction:

$$CuO + Fe_2O_3 + 4(NH_4)_2HPO_4 \longrightarrow CuFe_2(P_2O_7)_2 + 8NH_3\uparrow + 6H_2O\uparrow$$

The starting materials in powdered form were ground together and heated progressively up to 900 °C for 24 hours. For synthesis details see references [4,5].

Magnetic susceptibility measurements were carried out using a super-conducting quantum interference device (SQUID) magnetometer and the raw data were corrected for diamagnetism.

Neutron powder diffraction experiments were performed using the two-axis high-resolution powder diffractometer (G4-2) at the Laboratoire Léon Brillouin (LLB, Saclay-France) [6,7]. The G4-2 instrument uses a focusing germanium monochromator. The neutron wavelengths 1.80, 2.34 or 2.8 Å are available. The sample (about 6 g of powder) was put into a cylindrical vanadium can. A first measurement using the 1.80 Å wavelength was performed at room temperature. For the low temperature study the sample was inserted into a helium cryostat and several patterns, using neutrons of 2.343 Å wavelength, were collected between 1.4 and 20 K. The explored range of the scattering angle was 3–170°.

The refinement of powder diffraction data, in both paramagnetic and ordered states, was performed by the Rietveld method [8,9], using the program FULLPROF [10,11]. In order to refine the crystal structure we used as starting parameters those obtained by single crystal X-ray diffraction [4]. The magnetic structure was solved by a systematic search for solutions using the representation symmetry analysis method first introduced by Bertaut [12] and extensively developed by Izyumov and co-workers [13].

The analysis of the results was performed using some computer programs developed recently [1]. In particular the program SIMBO analyses the crystal structure of an insulator in terms of superexchange M_1–X–M_2 and super-superexchange M_1–X_1–X_2–M_2 paths. It needs as input the structural parameters, the ionic charge and the saturation magnetic moment of the different ions. The program use this information to calculate distances, angles and exchange paths. The program ENERMAG uses the output of SIMBO and calculates the classical magnetic energy as a function of the exchange interactions. It uses a generalisation of the Villain–Yoshimori theorem [14,15] for complex structures developed in the sixties by Lyons, Kaplan and Freiser [16,17]. ENERMAG is able to provide a magnetic phase diagram, for whatever topology, by calculating the first ordered state solving an eigenvalue problem (see below and appendix of reference [1]).

3. Results

3.1. Susceptibility measurements

The magnetic susceptibility measurements (Fig. 1) [5], show that the compound has an anti-ferromagnetic behaviour at low temperature. The analysis of the data gives a paramagnetic Curie temperature $\theta_p \approx -28$ K, and a Néel temperature $T_N \approx 16$ K. The paramagnetic moment per unit cell calculated for this compound is 8.54 μ_B which is in fair agreement with the experimental value deduced from the susceptibility data: 8.65 μ_B. The negative paramagnetic Curie temperature indicates predominant anti-ferromagnetic (AF) exchange interactions. A more detailed study of the susceptibility in terms of some assumptions about the kind of magnetic interactions existing in the compound is possible. Some of us started this study [5] using a simple model

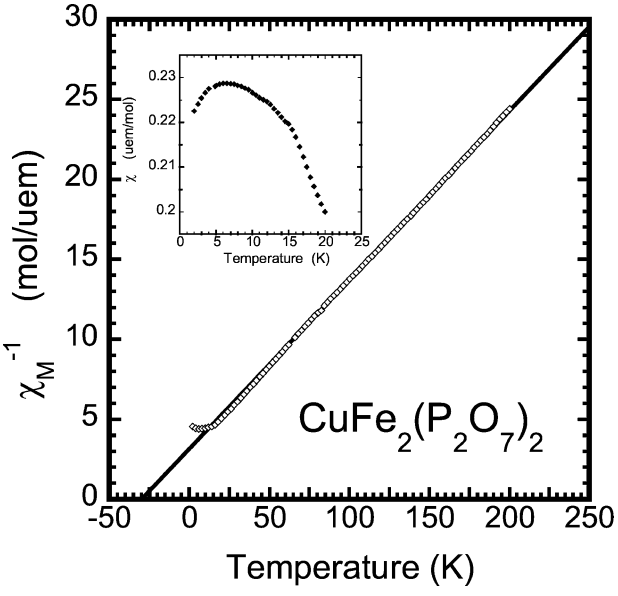

Fig. 1. $CuFe_2(P_2O_7)_2$ thermal variation of the reciprocal magnetic susceptibility (corrected for diamagnetism. Applied field: 2000 Oe). The continuous curve corresponds to the fit of the data using a Curie–Weiss law ($\frac{1}{\chi} = \frac{T-\theta}{C}$) in the paramagnetic region. In the inset it is shown the magnetic susceptibility versus temperature below 25 K.

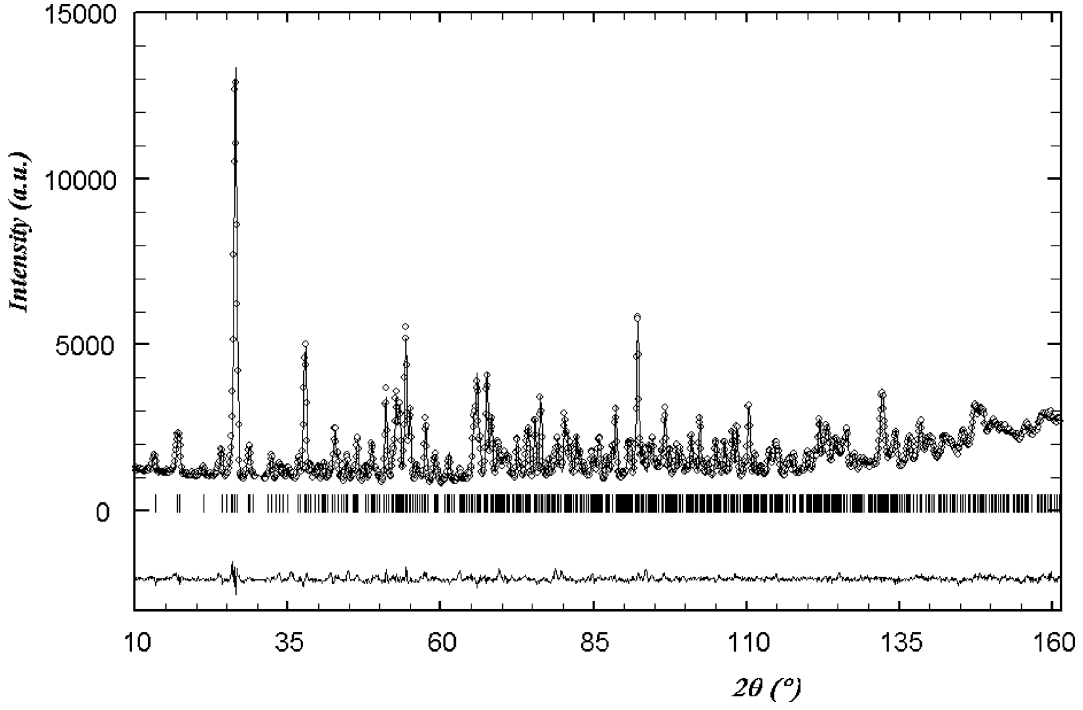

Fig. 2. Observed and calculated neutron powder diffraction patterns of $CuFe_2(P_2O_7)_2$ (room temperature, $\lambda = 1.80$ Å). Experimental points (○), calculated profile (—), position of nuclear peaks (|) and difference pattern (—). 34 structural parameters are refined for 733 reflections. $R_{\text{Bragg}} = 5.1\%$ and $\chi^2 = 3.0$. Some non indexed reflections belong to an unknown impurity and are excluded from pattern.

consisting of isolated clusters of three ions (the structural trimers: Fe–Cu–Fe) with an AF coupling between Cu and Fe. The trimers were treated exactly, using a single exchange constant $J_{\text{intra}} = J$(Cu–Fe), and the mean field approximation was used for treating the interaction between trimers using a phenomenological exchange constant J_{inter}. The fit in the paramagnetic region, and close to the transition temperature, was plausible and a superexchange constant $J_{\text{intra}} = -18$ K was obtained. We shall see below that this simple model is unable to explain the observed magnetic structure. This is a common situation where fitting susceptibility curves to an *a priori* model may give totally wrong results. The results of neutron diffraction experiments are clearly needed to complete, correct, discard or confirm the model fitting the susceptibility.

3.2. Crystal structure

The refinement of the pattern recorded at room temperature (Fig. 2) is in a good agreement with the monoclinic crystal structure determined by A. Boutfessi et al. [4]. The results of structure refinement are presented in Table 1.

The structure, described in [4], is shown in Fig. 3. The characteristic centrosymmetric trimers Fe–Cu–Fe are emphasized. The Fe^{3+} ions are magnetically connected with Cu^{2+} ions by near 90° superexchange paths in which the central Cu atoms, with square-planar coordination geometry, share two oxygen atoms with each of two neighbouring octahedrally coordinated Fe atoms. Trimers are connected through pyrophosphates groups P_2O_7.

A neutron powder diffraction diagram was measured at 20 K. The crystal structure parameters refined at room temperature is still adapted for the refinement of the diffraction pattern. We have then fixed the atom positions and refined only the profile parameters and those describing the magnetic structure.

3.3. Magnetic structure

The crystal structure of $CuFe_2(P_2O_7)_2$ does not change between room temperature and 20 K. Below 16.5 K some new diffraction peaks are observed in the neutron patterns. These peaks are due to magnetic ordering. Their intensity decreases with increasing temperature. Low angle parts of neutron diffraction patterns measured between 1.4 to 16.6 K are shown in Fig. 4. The magnetic reflections are indexed in the primitive monoclinic cell. The ordering is described by the propagation vector $\mathbf{k} = (1/2, 0, 1/2)$. The magnetic ions in the crystallographic lattice are Cu^{2+} and Fe^{3+} occupying the Wyckoff sites 2*a* and 4*e* (Table 2). The four one-dimensional irreducible representations of $P2_1/n$ space group and $\mathbf{k} = (1/2, 0, 1/2)$ are given in Table 3.

The best agreement between the calculated and the observed neutron diffraction pattern (measured below T_N) is obtained for the magnetic structure described by the representation Γ_2 with basis functions $[f_x(++), a_y(+-), f_z(++)]$ for position 2*a* and $[F_x, G_y, F_z]$ for position 4*e*. The symbols A(+−−+), C(++−−), F(++++), G(+−+−) correspond to Bertaut's [12] notations. The structure is well refined by using the collinear model [0, a_y, 0] [0, G_y, 0].

Table 1
Refined values of cell parameters, atomic positions and temperature factors for $CuFe_2(P_2O_7)_2$ at room temperature using 1.80 Å neutrons wavelength. Isotropic temperature factors of the same chemical species have been constrained to have the same values. The value of χ^2 is obtained only with points having contributions of Bragg reflections

Cell parameters					
Space group			$P2_1/n$		
a (Å)			6.5921(3)		
b (Å)			5.1606(2)		
c (Å)			15.6397(6)		
β (°)			91.983(3)		
V (Å^3)			531.73(12)		
Atom		Atomic positions			
		x	y	z	B (Å^2)
Cu	2a	0	0	0	0.88(11)
Fe	4e	0.3344(5)	0.2423(9)	0.1199(2)	0.71(6)
P2	4e	0.3544(9)	0.2754(13)	−0.0949(4)	0.55(7)
P1	4e	−0.0501(8)	0.2529(15)	−0.1688(3)	0.55(7)
O21	4e	0.2452(9)	0.2076(12)	−0.0134(4)	1.15(4)
O11	4e	0.1902(9)	0.2838(12)	−0.1697(4)	1.15(4)
O12	4e	−0.0811(8)	−0.0021(13)	−0.1204(4)	1.15(4)
O13	4e	−0.1320(9)	0.4755(12)	−0.1178(4)	1.15(4)
O14	4e	−0.1299(9)	0.2253(13)	−0.2578(4)	1.15(4)
O22	4e	0.5080(9)	0.0828(11)	−0.1178(4)	1.15(4)
O23	4e	0.4354(9)	0.5528(11)	−0.0867(4)	1.15(4)
Conditions of refinement					
Refined domain			[5.0°, 29.1] ∪ [30.4, 160.8°]		
Number of reflections			733		
Structural parameters			34		
Bragg R-factor (%)			5.1		
χ^2			3.0		
R_{WP} (%)			5.17		
R_P (%)			3.97		

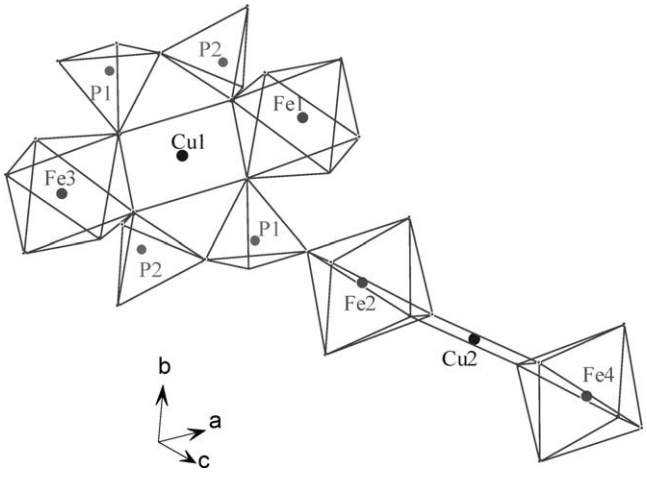

Fig. 3. Schematic representation of polyhedra CuO_4, FeO_6 and PO_4 present in the crystal structure of $CuFe_2(P_2O_7)_2$. Two FeO_6–CuO_4–FeO_6 trimers are represented showing two different orientations. The numbering of atoms is that used for the magnetic structure analysis.

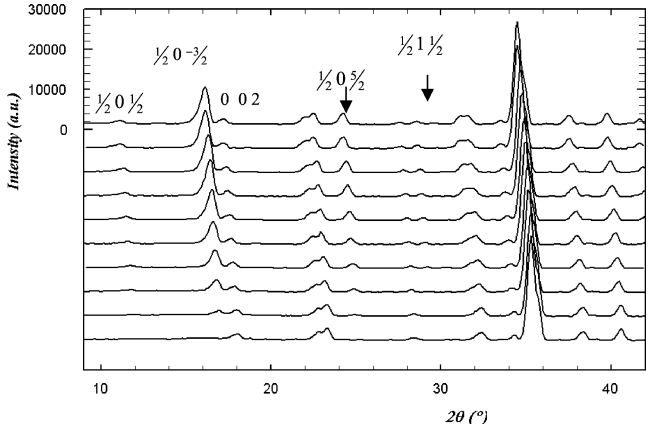

Fig. 4. Low angle part of the neutron powder diffraction patterns (λ = 2.343 Å) of $CuFe_2(P_2O_7)_2$ at temperatures 1.4; 1.9; 2.5; 2.8; 5.7; 8.6; 10.6; 12.6; 14.6 and 16.6 K. The intensity of magnetic peaks progressively increases on going to low temperatures.

This magnetic model was used to refine all the neutron diffraction patterns measured for temperatures below 16.6 K. The example of 1.4 K is shown in Fig. 5 and the corresponding refined parameters are listed in Table 4. The calculated magnetic moments of Cu^{2+} and Fe^{3+} are along the b axis (Fig. 6). The moments of atoms belonging to a same trimer have same direction. The ordering within the trimer is then ferromagnetic. Neighbouring trimers have opposite orientations along a and c axis. The ordering between trimers is anti-ferromagnetic. The refined values of magnetic moments at 1.4 K are 0.83(6) μ_B for Cu^{2+}

Table 2
$CuFe_2(P_2O_7)_2$: positions of magnetic atoms in the crystallographic cell and the corresponding values of magnetic moments at 1.4 K. See Table 1 for the specific values of (x, y, z) for Fe1 position

Atoms	Atomic positions			Magnetic moments (μ_B)		
	x	y	z	M_x	M_y	M_z
Cu1	0	0	0	0	−0.83 (6)	0
Cu2	1/2	1/2	1/2	0	0.83 (6)	0
Fe1	x	y	z	0	−4.88 (4)	0
Fe2	$1/2-x$	$1/2+y$	$1/2-z$	0	4.88 (4)	0
Fe3	$1-x$	$1-y$	$1-z$	0	−4.88 (4)	0
Fe4	$1/2+x$	$1/2-y$	$1/2+z$	0	4.88 (4)	0

Table 3
Irreducible representations of $P2_1/n$ space group for propagation vector $\mathbf{k} = (1/2, 0, 1/2)$. The basis functions corresponding to the Wyckoff positions 2*a* and *4e* describe possible magnetic structures for $CuFe_2(P_2O_7)_2$. The two signs (+) and (−) correspond to the sign of the magnetic moments components along **a**, **b**, and **c** cell axis. The sequence of atoms is given in Table 2. The area in a frame corresponds to the observed magnetic structure

Irreducible representations	Symmetry operations				Cu^{2+}			Fe^{3+}		
	1	$2_1 y$	−1	n	x	y	z	x	y	z
Γ_1	1	1	1	1	$a_x(+-)$	$f_y(++)$	$a_z(+-)$	G_x (+−+−)	F_y (++++)	G_z (+−+−)
Γ_2	1	−1	1	−1	$f_x(++)$	$a_y(+-)$	$f_z(++)$	F_x (++++)	G_y (+−+−)	F_z (++++)
Γ_3	1	1	−1	−1	0	0	0	A_x (+−−+)	C_y (++−−)	A_z (+−−+)
Γ_4	1	−1	−1	1	0	0	0	C_x (++−−)	A_y (+−−+)	C_z (++−−)

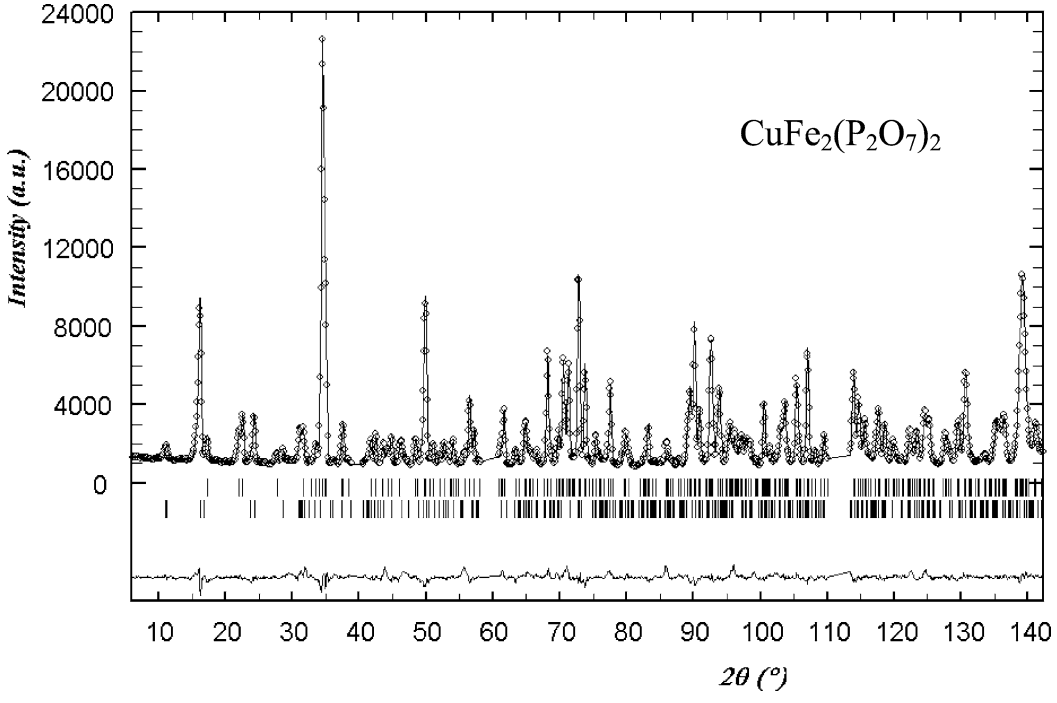

Fig. 5. Observed (○) versus calculated (—) neutron powder diffraction pattern (λ = 2.343 Å) of $CuFe_2(P_2O_7)_2$ at 1.4 K. Nuclear (first row) and magnetic (second row) reflections positions are represented by vertical bars (|). We have refined 12 structural parameters for 280 nuclear reflections and 546 magnetic reflections. The relevant reliability indices are R_{Bragg}(nuclear) = 4.6%, R_{Bragg}(magnetic) = 8.6%, $\chi^2 = 7.9$.

and 4.88(4) μ_B for Fe^{3+}. The fit of the evolution of magnetic moments versus temperature (Fig. 7) leads to a Néel temperature $T_N = (15.5 \pm 0.5)$ K. The Cu^{2+} ($3d^9$) ion, located in a square site, has a $t_{2g}^6 e_g^3$ electronic configuration with a single electron (hole) on the $d_{x^2-y^2}$ orbital. The saturation magnetic moment (spin-only) of the free ion is 1 μ_B. The Fe^{3+} ($3d^5$) ion is located in an octahedral site, with five single electrons in $t_{2g}^3 e_g^2$ configuration. The magnetic moment of the free ion in high spin configuration is 5 μ_B. The observed magnetic moments agree well with what is expected from the free ion values. The reduction with respect to the spin-only values of the free ions is normally due to a combination of covalence effects and zero-point spin fluctuations in antiferromagnets.

Table 4
Cell parameters and reliability indices of $CuFe_2(P_2O_7)_2$ obtained by refinement of the neutron powder diffraction patterns ($\lambda = 2.343$ Å) measured at 1.4 K. The structural parameters have been fixed to the values found in the paramagnetic state. Excluded regions contain peaks of an unknown impurity

Structural parameters		Analysis of the refinement	
a (Å)	6.5845(2)	Refinement domain	[6; 38.9°] ∪ [40.4; 58.2] ∪ [60.7; 110.0] ∪ [113.3; 142.3]
b (Å)	5.1555(2)	Number of reflections	nuclear phase: 280; magnetic phase: 543
c (Å)	15.6189(4)	Number of free parameters	11
α (°)	90.0	Bragg R-factor (%)	4.6
β (°)	91.994(2)	Magnetic R-factor (%)	8.6
γ (°)	90.0	χ^2	7.9

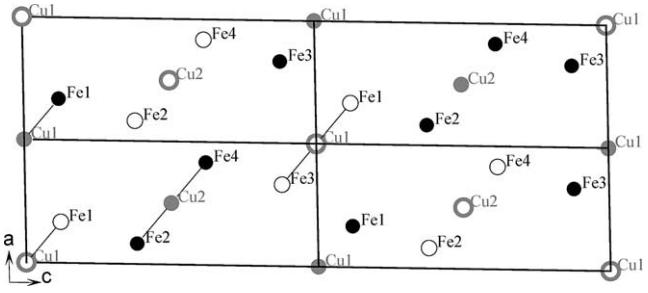

Fig. 6. Projection, in ac plane, of magnetic structure of $CuFe_2(P_2O_7)_2$ compound; open and closed symbols represent parallel and anti-parallel magnetic moments, respectively, to b axis. The same rule for the representation of the magnetic moments orientation is valid for Figs. 8 and 9.

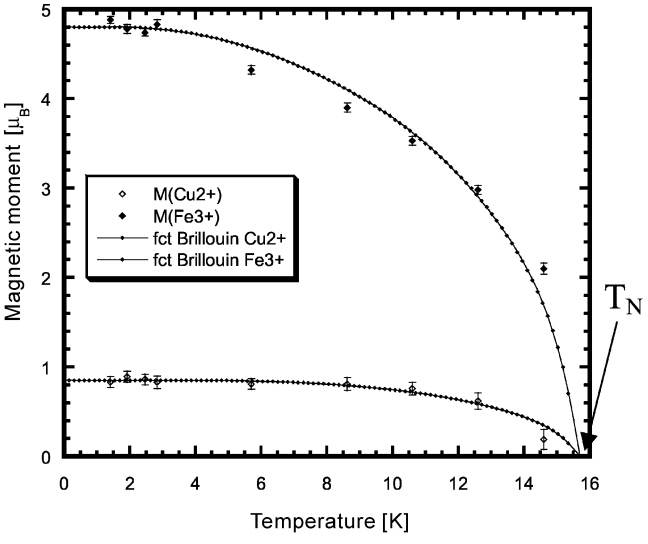

Fig. 7. Temperature variation of magnetic moments of Cu^{2+} and Fe^{3+} in $CuFe_2(P_2O_7)_2$. The continuous curve is a Brillouin function fitting providing $T_N = 15.5$ K, $M_0(\mathrm{Cu}) = 0.85\ \mu_B$ and $M_0(\mathrm{Fe}) = 4.80\ \mu_B$.

4. Magnetic phase diagram

There is no other magnetic transition observed below 15.5 K, so that the first ordered state characterised by the propagation vector $\mathbf{k} = (1/2, 0, 1/2)$ corresponds to the magnetic ground state. Theoretically, the first ordered state is obtained, as a function of $\mathbf{k}$, on the surface or at the interior of the Brillouin Zone (BZ), and the exchange integrals, as the eigenvector corresponding to the lowest eigenvalue of the negative Fourier transform of exchange integral matrix [14–17]:

$$\boldsymbol{\xi}_{ij}(\mathbf{k}) = -\sum_m J_{ij}(\mathbf{R}_\mathrm{m}) \cdot \exp\{-2\pi \mathrm{i}\, \mathbf{k}\mathbf{R}_\mathrm{m}\}.$$

The indices i, j refer to the magnetic atoms in a primitive cell, $J_{ij}(\mathbf{R}_\mathrm{m})$ is the isotropic exchange interaction between the spins of atoms i and j in unit cells separated by the lattice vector $\mathbf{R}_\mathrm{m}$. We have adopted the interaction energy between two spins as $W = -\mathrm{J}_{ij}\mathbf{S}_i\mathbf{S}_j = -\mathrm{J}_{ij}\mathrm{S}_i\mathrm{S}_j\mathbf{s}_i\mathbf{s}_j = -J_{ij}\mathbf{s}_i\mathbf{s}_j$, so the exchange interaction written in the expression of $\boldsymbol{\xi}_{ij}(\mathbf{k})$, contains implicitly the magnitudes of the spins. The energy, λ, lowest eigenvalue of the matrix $\boldsymbol{\xi}(\mathbf{k}, \{J_{ij}\})$, as a function of the exchange integrals and $\mathbf{k} = (X, Y, Z)$ can be obtained numerically. The vector $\mathbf{k}$ minimising $\lambda(\mathbf{k}, \{J_{ij}\})$ for a given set of $\{J_{ij}\}$ is the propagation vector of the magnetic structure and the spin configuration is obtained from the corresponding eigenvector [14–17]. If for a particular $\mathbf{k}$ vector we obtain degeneracy (same value) of two eigenvalues, the magnetic structure correspond to an arbitrary linear combination of the two eigenvectors. This is the case of non-collinear magnetic structures resulting from the competition of isotropic interactions. For the cases in which $\mathbf{k} = 1/2\mathbf{H}$, being $\mathbf{H}$ a reciprocal lattice vector, including $\mathbf{H} = (0, 0, 0)$, the eigenvectors are all real and the sequence of signs of the eigenvector components corresponding to the lowest eigenvalue, gives the spin configuration corresponding to the first ordered state, which is also the ground state in our particular case. We consider only isotropic exchange interactions to study the main characteristics of the magnetic ordering. The anisotropy terms of the Hamiltonian (anisotropic symmetric and antisymmetric exchange and single-ion anisotropy) act as a perturbation fixing the orientation of the spins with respect to the crystallographic lattice.

We first need to identify the M–M′ interactions in $CuFe_2(P_2O_7)_2$, where M and M′ symbolise a magnetic ion (Cu^{2+} or Fe^{3+}). Magnetic exchange is supposed to be isotropic and described by the exchange constants J_i, where "i" is an integer number increasing with distance linking M and M′. We used the program SIMBO to determine the independent number of possible exchange interaction occurring in the magnetic topology of $CuFe_2(P_2O_7)_2$. As a result, a complete listing of interactions between magnetic ions within a 5.2 Å range is given in Table 5. The magnetic ions interact by super or super-superexchange mediated by oxygen ions, all of them belong to PO_4 tetrahedra. A comment

Table 5
Exchange interactions connecting transition elements in $CuFe_2(P_2O_7)_2$ structure within a distance range of 5.2 Å. Interaction path, bond lengths (approximated to a hundredth of 1 Å), and relevant exchanges angles (approximated to one degree) are given. For superexchange path of the form M–O–M′, the geometrical parameters are given in the following order: distance M–O, distance O–M′, superexchange angle M–O–M′, sum of bond distances M–O and O–M′ (in bold). For super-superexchange path of the form M–O–O′-M′, the geometrical parameters are given in the following order: distance M–O, distance O–O′, distance O′–M′, angle M–O–O′, angle O–O′–M′, torsion angle M–O–O′–M′ (underlined), sum of bond distances M–O, O–O′ and O′–M′ (in bold)

Interaction	Description	Representative exchange path	Distance (Å)	Distances (Å), angles (°), torsion angle (°), total bond's length (Å)	Remarks
1: J_1: Cu–Fe	Superexchange between CuO_4 and FeO_6 sharing an edge. J_1 is the intra-trimer interaction.	Cu–O21–Fe Cu–O12–Fe	3.11	1.96, 2.15, 98, **4.11** 1.94, 2.08, 101, **4.02**	Exchange angles are 98° and 101°, exchange probably weakly ferromagnetic, $J_1 > 0$.
2: J_2: Cu–Fe	Super-superexchange via the edge of a PO_4 tetrahedron. Cu^{2+} and Fe^{3+} belong to two different trimers related by the translation [010]. A part of the path is common to the path of interaction **7**. Two trimers along [010] are connected by two interactions of type **2** and two interactions of type **7**.	Cu–O12–O13–Fe	4.84	1.94, 2.49, 1.97, 91, 145, 107, **6.40**	Angles are equal to 91° and 145; first one corresponds to a ferromagnetic exchange and second one to an antiferromagnetic exchange. Torsion angle equal to 107° points to a weak interaction of uncertain sign.
3: J_3: Fe–Fe	Interaction connecting two Fe^{3+} ions by two super-superexchange paths. Fe^{3+} ions belong to different trimers having the central copper are at positions (x, y, z) and $(x + 1/2, y + 1/2, z + 1/2)$ or $(x - 1/2, y - 1/2, z - 1/2)$. Each Fe^{3+} participates in two interactions (J_3) with two different Fe^{3+} ions.	Fe–O12–O14–Fe Fe–O14–O13–Fe	4.98	2.08, 2.46, 1.93, 102, 157, 59, **6.46** 1.93, 2.54, 1.97, 144, 113, 35, **6.44**	Superexchange angles are 102° and 157° for one path, 144° and 113° for the other one. Sign of the interaction uncertain.
4: J_4: Cu–Fe	Describes the interaction between Cu^{2+} and Fe^{3+} ions belonging to two trimers with central coppers separated by the translation [100]. Each trimer is associated to two interactions (J_4) with trimers at a distance "a".	Cu–O21–O22–Fe	4.99	1.96, 2.51, 1.97, 121, 127, 60, **6.44**	Similar exchange angles: 121 and 127°. Interaction of probable negative sign.
5: J_5: Fe–Fe	Interaction connecting two Fe^{3+} ions through a double super-superexchange bridge. Central coppers of the trimers are separated by the translation [100].	Fe–O21–O22–Fe Fe–O22–O21–Fe	5.07	2.15, 2.51, 1.97, 119, 127, 62, **6.63** 1.97, 2.51, 2.15, 127, 119, 62, **6.63**	Two equivalent paths. Exchange angles are similar (119 and 127°). Interaction of probable negative sign.
6: J_6: Fe–Fe	Interaction connecting through a double super-superexchange bridge two Fe^{3+} ions belonging to different trimers. The Cu atoms of trimers are separated by the translation [110].	Fe–O21–O23–Fe Fe–O23–O21–Fe Fe–O23–O23–Fe	5.15	2.15, 2.48, 1.94, 105, 158, 52, **6.57** 1.94, 2.48, 2.15, 158, 105, 52, **6.57** 1.94, 2.87, 1.94, 99, 99, 0, **6.74**	Two equivalent paths connect Fe^{3+} ions. Sign of the interaction uncertain.
7: J_7: Fe–Fe	Interaction connecting two Fe^{3+} ions along [010] through two simultaneous super-superexchange paths. Each Fe^{3+} participates in two interactions **7**.	Fe–O12–O13–Fe Fe–O22–O23–Fe	5.16	2.08, 2.49, 1.97, 119, 145, 4, **6.54** 1.97, 2.52, 1.94, 158, 109, 46, **6.43**	A double super-superexchange path through two PO_4 tetrahedron edges. Interaction of probable negative sign.
8: J_8: Cu–Cu	Interaction between two Cu^{2+} along [010].	no super-superexchange path	5.16		Neglected interaction.

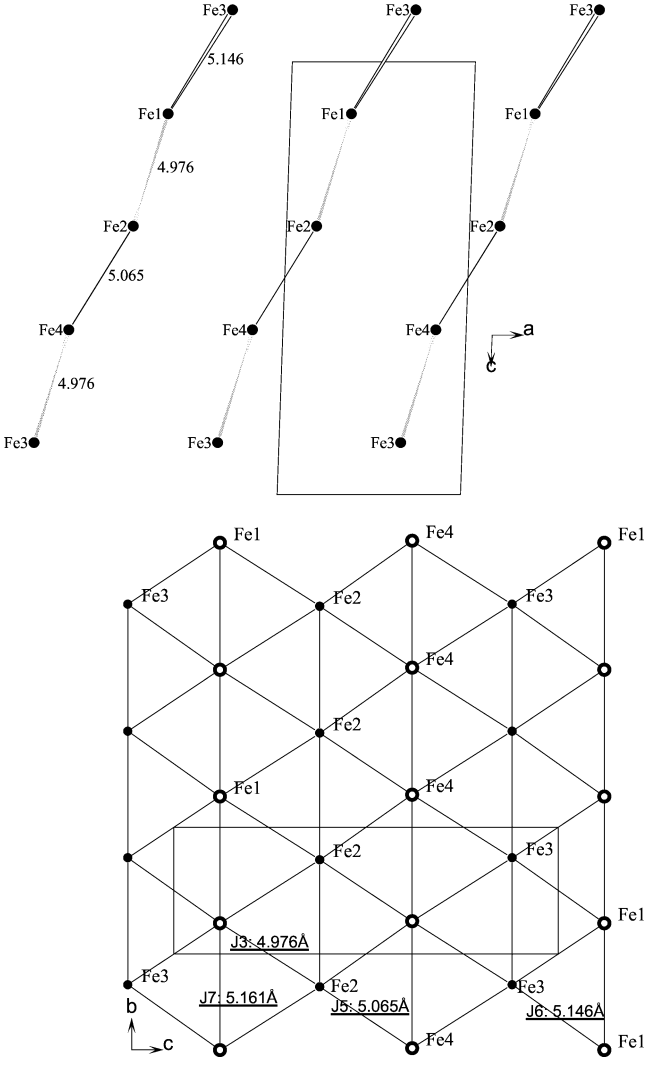

Fig. 8. The Fe^{3+}-ions in $CuFe_2(P_2O_7)_2$ are disposed within parallel puckered triangular layers holding the interactions numbered **3**, **5**, **6** and **7**. Projection in plane *ac* (top), showing the distorted triangular layers. The projection in *bc* plane (bottom) shows explicitly the pattern of interactions.

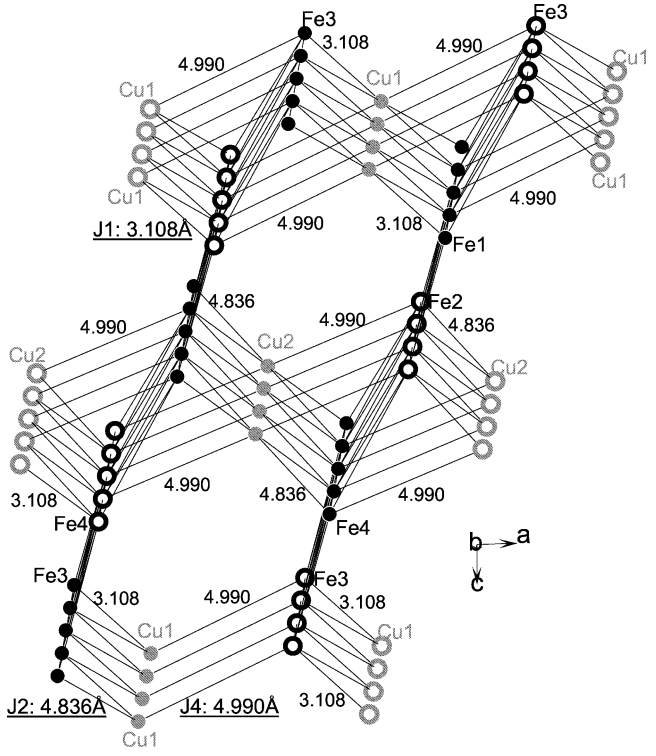

Fig. 9. Relative positions of $\ldots Fe^{3+}$–$Fe^{3+}\ldots$ layers and Cu^{2+}-ions in the magnetic topology of $CuFe_2(P_2O_7)_2$. The interactions numbered **3**, **5**, **6** and **7** occur inside the layer, whereas the layers are linked via the interactions **1**, **2**, and **4** connecting Cu^{2+} and Fe^{3+} ions.

concerning the predicted sign of the exchange interactions according to the Goodenough–Kanamori–Anderson rules is also included in the last column of Table 5.

The interactions numbered **1**, **2**, and **4** (characterised by J_1, J_2 and J_4 exchange constants) connect Cu^{2+} and Fe^{3+} ions by a superexchange path involving a single bridging oxygen (J_1) of by super-superexchange through a PO_4 tetrahedron (J_2, J_4). In interaction **1**: d(Cu^{2+}–Fe^{3+}) = 3.11 Å, Cu^{2+} and Fe^{3+} belong to the same trimer Fe–Cu–Fe, but the magnetic ions associated to the interactions **2**: d(Cu^{2+}–Fe^{3+}) = 4.84 Å, and **4**: d(Cu^{2+}–Fe^{3+}) = 4.99 Å, belong to different Fe–Cu–Fe trimers. The interactions numbered by **3**, **5**, **6** and **7** connect only Fe^{3+} ions belonging to different trimers and all these interactions link Fe^{3+} ions belonging to a same triangular layer, as it is displayed in Fig. 8. The Fe^{3+} ions in triangular layers are connected, through interactions **3**: d(Fe^{3+}–Fe^{3+}) = 4.98 Å, **5**: d(Fe^{3+}–Fe^{3+}) = 5.07 Å, **6**: d(Fe^{3+}–Fe^{3+}) = 5.15 Å, and **7**: d(Fe^{3+}–Fe^{3+}) = 5.16 Å. The layers are nearly parallel to the (101) planes (Fig. 8). The minimal distance separating two consecutive layers (d_{min} = 6.216 Å) is the distance Fe–Fe in a same trimer (Fig. 9). The interaction **8**: d(Cu^{2+}–Cu^{2+}) = 5.16 Å has been neglected because there is no super-superexchange path, with Cu–O–O′ angle larger than 90°, between the two Cu^{2+} ions related by the translation [010]. The distances separating magnetic ions for interactions **2** to **7** vary in an sharp interval of 0.325 Å. Superexchange angles in the corresponding exchange paths are also similar. This means that the evaluation criteria for the relative strength of interactions **2** to **7** is very difficult to establish.

If we consider a larger range of distances (say 8 Å), we obtain a gap of 1 Å between the last already described interaction and the next one connecting Cu^{2+} and Fe^{3+} at a distance of 6.15 Å. We have then discarded all interactions between M and M′ separated by more than 5.2 Å.

To study the problem with the program ENERMAG we can consider the exchange interactions J_i ($i = 2, \ldots, 7$), taking J_1 as a reference value ($J_1 = 1$ or $J_1 = -1$), as varying J_i in the interval $[-20, 20]$ and the **k**-vectors inside, and in special points, of the BZ. However, the number of free parameters (6 exchange parameters) is too high. To get some insight into the conditions to be satisfied by the exchange interactions, in order to get the calculated first ordered state identical to the observed magnetic structure, we have to reduce this too large number of parameters. The

Table 6
$CuFe_2(P_2O_7)_2$: magnetic exchange matrix. The primitive cell contain six magnetic atoms. Different exchange interactions are numbered up to 6.0 Å by increasing distance: J_1, J_2, J_3, J_4, J_5, J_6, J_7 and J_8 (see text). We considered $J_8 = 0$ because there is no super-superexchange path connecting the extreme atoms

$$\xi(\mathbf{k}, J_{ij}) = \begin{array}{c} \\ \text{Cu(1)} \\ \text{Cu(2)} \\ \text{Fe(1)} \\ \text{Fe(2)} \\ \text{Fe(2)} \\ \text{Fe(2)} \end{array} \begin{array}{c} \begin{array}{cccccc} \text{Cu(2)} & \text{Cu(2)} & \text{Fe(1)} & \text{Fe(2)} & \text{Fe(3)} & \text{Fe(4)} \end{array} \\ \begin{pmatrix} 0 & 0 & \xi_{13} & 0 & \xi_{15} & 0 \\ 0 & 0 & 0 & \xi_{24} & 0 & \xi_{26} \\ \xi_{31} & 0 & \xi_{33} & \xi_{34} & \xi_{35} & 0 \\ 0 & \xi_{42} & \xi_{43} & \xi_{44} & 0 & \xi_{46} \\ \xi_{51} & 0 & \xi_{53} & 0 & \xi_{55} & \xi_{56} \\ 0 & \xi_{62} & 0 & \xi_{64} & \xi_{65} & \xi_{66} \end{pmatrix} \end{array}$$

with: $\begin{cases} \mathrm{A} = \mathrm{e}^{2\pi \mathrm{i}\, \mathrm{X}} \\ \mathrm{B} = \mathrm{e}^{2\pi \mathrm{i}\, \mathrm{Y}} \\ \mathrm{C} = \mathrm{e}^{2\pi \mathrm{i}\, \mathrm{Z}} \end{cases}$

X, Y and Z are the propagation vector components, $\mathbf{k} = (X, Y, Z)$, in reciprocal space.

Exchange matrix:

$$\xi(\mathbf{k}, J_{ij}) = \begin{pmatrix} 0 & 0 & J_1 + J_2 B + J_4 A & 0 & J_1\mathrm{ABC} + J_2\mathrm{AC} + J_4\mathrm{BC} & 0 \\ 0 & 0 & 0 & J_1 + J_2\mathrm{B} + J_4\mathrm{A}^* & 0 & J_1 + J_2\mathrm{B}^* + J_4\mathrm{A} \\ J_1 + J_2\mathrm{B}^* + J_4\mathrm{A}^* & 0 & J_7\ (\mathrm{B} + \mathrm{B}^*) & J_3\ (1 + \mathrm{B}) & J_5\mathrm{BC} + J_6\mathrm{C} & 0 \\ 0 & J_1 + J_2\mathrm{B}^* + J_4\mathrm{A} & J_3\ (1 + \mathrm{B}^*) & J_7\ (\mathrm{B} + \mathrm{B}^*) & 0 & J_5\mathrm{A} + J_6\mathrm{AB}^* \\ J_1\mathrm{A}^*\mathrm{B}^*\mathrm{C}^* + J_2\mathrm{A}^*\mathrm{C}^* + J_4\mathrm{B}^*\mathrm{C}^* & 0 & J_5\mathrm{B}^*\mathrm{C}^* + J_6\mathrm{C}^* & 0 & J_7(B + \mathrm{B}^*) & J_3(1 + \mathrm{B}^*) \\ 0 & J_1 + J_2\mathrm{B} + J_4\mathrm{A}^* & 0 & J_5\mathrm{A}^* + J_6\mathrm{A}^* B & J_3(1 + \mathrm{B}) & J_7(\mathrm{B} + \mathrm{B}^*) \end{pmatrix}$$

Table 7
Sequence of magnetic moments orientation along one direction (collinear case) for the topology of $CuFe_2(P_2O_7)_2$ for atoms Cu_1, Cu_2, Fe_1, Fe_2, Fe_3 and Fe_4 (atomic positions given in Table 2). The magnetic structure numbered 6 correspond to the experimental ground state. The number associated to each magnetic configuration are used for describing the different areas in the J-space of the magnetic phase diagram (see figure)

Propagation vector	Sequences of magnetic moment signs along an arbitrary axis					
	M_{Cu1}	M_{Cu2}	M_{Fe1}	M_{Fe2}	M_{Fe3}	M_{Fe4}
1: $\mathbf{k} = (0, 0, 0)$	+	+	+	+	+	+
2: $\mathbf{k} = (0, 0, 0)$	+	+	−	−	−	−
3: $\mathbf{k} = (0, 0, 0)$	+	−	+	−	+	−
4: $\mathbf{k} = (1/2, 0, 1/2)$	+	+	+	+	+	+
5: $\mathbf{k} = (1/2, 0, 1/2)$	+	+	−	−	−	−
6: $\mathbf{k} = (1/2, 0, 1/2)$	+	−	+	−	+	−
7	no order or incommensurate non-collinear structures					

hypothesis we have considered is that the interactions **3**, **5**, **6** and **7**, connecting Fe^{3+} ions within a same layer, are all equivalent. We have then considered in our calculations that $J_3 = J_5 = J_6 = J_7 = J_{3,5,6,7}$. The exchange interaction matrix as provided by the program SIMBO and used by ENERMAG is written in complete form in Table 6. Taking a broader range than $[-20, 20]$ for the exchange interactions does not change qualitatively the results. One can deduce, by continuity, the shape of the phase diagram for regions outside the used range in the numerical calculations. All exchange interactions are then effectively measured in units of $|J_1|$. An auxiliary program takes the output of ENERMAG and plots a high dimensional phase diagram using the exchange interactions as Cartesian axes. The different regions correspond to different magnetic structures. We have numbered the six kinds of collinear magnetic structures found by the program and numbered as "7" the regions where either there is no classical magnetic order (degeneracy of the magnetic energy with respect to the value of **k**) or the magnetic structure is incommensurate due to strong frustrations effects. In Table 7 it is represented the sign sequence characterising the six collinear structures. The magnetic structure experimentally observed for the compound $CuFe_2(P_2O_7)_2$ is numbered as "6" in Table 7 and it is described by the sequence $\{\mathbf{k} = (1/2, 0, 1/2)$: $(+ - + - + -)\}$.

Table 8
Conditions to be satisfied by the exchange interaction to get the magnetic structure n°6 as the magnetic ground state (Table 7) experimentally observed in $CuFe_2(P_2O_7)_2$

Domain of interaction constants giving rise to structure n°6 in the magnetic phase diagram
$J_1 > 0$
$J_2 > J_1$
$J_{3,5,6,7} < 0 \quad (\lvert J_{3,5,6,7} \rvert \sim J_1)$
$J_4 + J_1 < 0$

In Fig. 10 we have represented 2D maps of different regions of the magnetic phase diagram for representative cases. The obtained magnetic phase diagram shows large domains without any magnetic ordering or dominated by incommensurate magnetic structures, mainly for $J_{3,5,6,7} < 0$, where frustration in the triangular network dominates over the rest of exchange interactions. An analysis of the boundaries between the regions gives us the conditions that have to satisfy the exchange integrals to give, as the first ordered state, the observed magnetic structure. In our case the region "6" requires that exchange interactions verify the constraints displayed in Table 8.

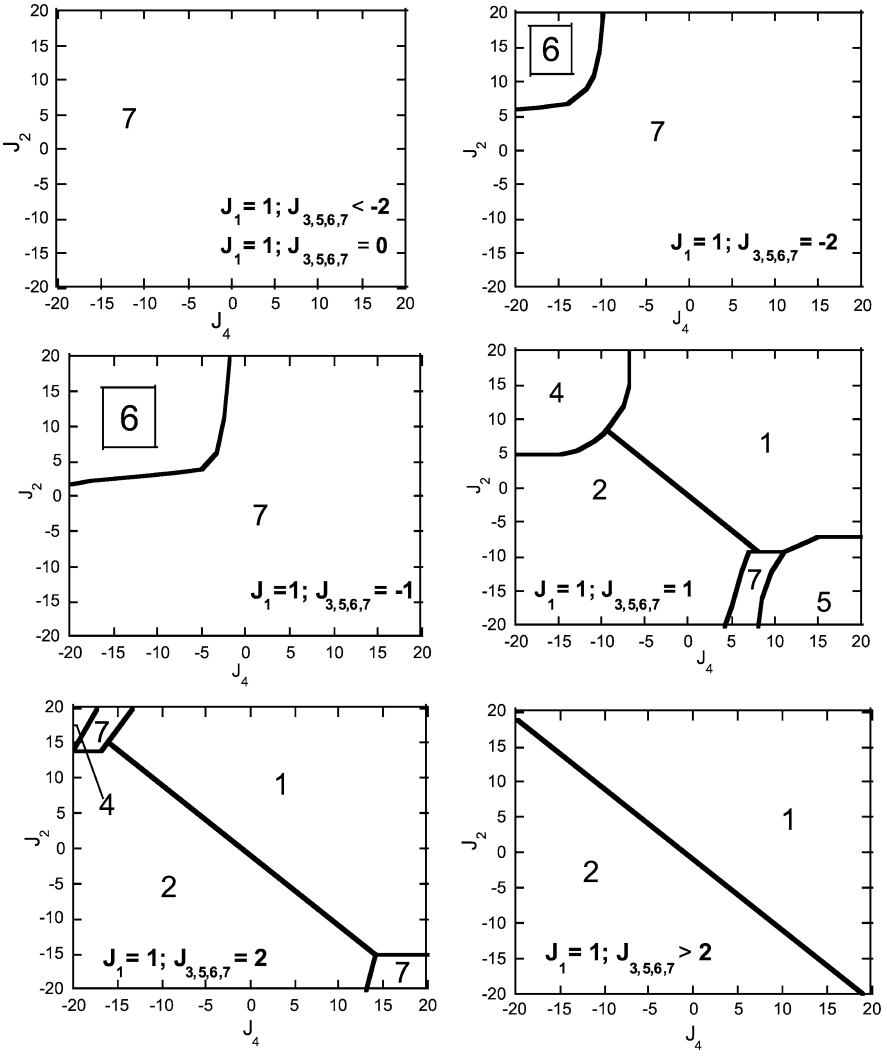

Fig. 10. Selected sections of the magnetic phase diagram of $CuFe_2(P_2O_7)_2$. The exchange constant J_1 has been taken as unity ($J_1 = 1$). To simplify the analysis we have taken as equal all exchange interactions within the triangular layers ($J_3 = J_5 = J_6 = J_7 = J_{3,5,6,7}$). A systematic variation of J_2, $J_{3,5,6,7}$ and J_4 constants in the domain $[-20, 20]$ by a step equal to 1 has been used to generate the phase diagram by using ENERMAG. The different magnetic structures numbered from 1 to 7 are described explicitly in Table 7. The observed magnetic structure correspond to domain 6.

Considering the magnetic ordering in the Fe^{3+} network, particularly within a triangular layer, we observe the alternation of ferromagnetic ordered rows (Figs. 6, 8, 9), parallel to [010], coupled antiferromagnetically. Triangular layers are parallel to [010], so that the system minimises frustration by using an alternating antiferromagnetic configuration and satisfying the interactions linking layers through Cu^{2+} ions.

5. Conclusions

We have solved and refined the magnetic structure of the pyrophosphate $CuFe_2(P_2O_7)_2$. There is no structural or magnetic phase transition below room temperature. The Néel temperature is $T_N = 15.5$ (5) K and there is no spin reorientation or magnetic phase transition below T_N.

The magnetic ions inside a Fe–Cu–Fe trimer order ferromagnetically. The trimers are ordered antiferromagnetically according to the propagation vector $\mathbf{k} = (1/2, 0, 1/2)$. The magnetic exchange interactions between magnetic ions are numerous and complex. We have considered effective exchange interactions within a sphere of radius 6 Å around all magnetic atoms. Apart from the Fe–Cu–Fe trimers, involving superexchange interactions, the most prominent aspect of the magnetic topology of $CuFe_2(P_2O_7)_2$, is the presence of distorted triangular layers of Fe^{3+} ions. The Fe^{3+}–Fe^{3+} interactions are of the super-superexchange type and of weak antiferromagnetic character. These layers are parallel and are connected through Fe–O–Cu–O′–Fe′ interactions. The interactions connecting iron layers are positive for cases **1** and **2** and negative for case **4**. The intrinsic frustration of triangular layers is released globally by the balance with other exchange interactions of ferromagnetic character between the layers. However, the observation of the structure "6" {$\mathbf{k} = (1/2, 0, 1/2)$: $(+-+-+-)$} in the domain $J_{3,5,6,7} < 0$ implies that the

spin arrangement in the triangular layers does not satisfy all the interactions and the spin configuration is partially frustrated.

Acknowledgements

The authors thank J. Darriet of the Institut de Chimie de la Matière Condensée de Bordeaux for the susceptibility measurements. This research has been supported by the institutions CEA-DRI (France), CNESTEN (Morocco) and COPEP.

References

[1] N. El Khayati, R. Cherkaoui El Moursli, J. Rodríguez-Carvajal, G. André, N. Blanchard, F. Bourée, G. Collin, T. Roisnel, The European Physical Journal B 22 (2001) 429.
[2] G. Rousse, J. Rodríguez-Carvajal, C. Wurm, C. Masquelier, Chemistry of Materials 13 (2001) 4527.
[3] G. Rousse, J. Rodríguez-Carvajal, C. Wurm, C. Masquelier, Solid State Sciences 4 (2002) 973.
[4] A. Boutfessi, A. Boukhari, E.M. Holt, Acta Crystallogr., Sect. C 52 (1996) 1597.
[5] A. Boutfessi, Thesis, Faculté des Sciences de Rabat (1999).
[6] The characteristics of the diffractometer G4.2 may be found at the Web site of the LLB: http://www-llb.cea.fr.
[7] A.I. Kurbakov, V.A. Trunov, T.K. Baranova, A.P. Bulkin, R.P. Dmitriev, Ya.A. Kasman, J. Rodríguez-Carvajal, T. Roisnel, Russian–French High Resolution Multi-Section Neutron Powder Diffractometer, Materials Science Forum 321–324 (2000) 308.
[8] H.M. Rietveld, Acta Crystallogr. 22 (1967) 151.
[9] H.M. Rietveld, J. Appl. Cryst. 2 (1969) 65.
[10] J. Rodríguez-Carvajal, Physica B 192 (1993) 55.
[11] J. Rodríguez-Carvajal, T. Roisnel, FullProf.98 and WinPLOTR New Windows95/NT Applications for Diffraction, IUCr Comm. Powder Diffract. Newsletter 20 (1998) 35.
[12] E.F. Bertaut, Acta Crystallogr., Sect. A 24 (1968) 217.
[13] Yu.A. Izyumov, V.E. Naish, R.P. Ozerov, Neutron Diffraction of Magnetic Materials, Consultants Bureau, New York, 1991.
[14] A. Yoshimori, J. Phys. Soc. Japan 14 (1959) 807.
[15] J. Villain, J. Phys. Chem. Solids 11 (1959) 303.
[16] D.H. Lyons, T.A. Kaplan, Physical Review 120 (1960) 1580.
[17] M.J. Freiser, Phys. Rev. 123 (1961) 2003.